Separation and Purification Technology 282 (2022) 120125

Contents lists available at ScienceDirect

Separation and Purification Technology

journal homepage: www.elsevier.com/locate/seppur

Advanced descriptors for long-range noncovalent interactions between SARS-CoV-2 spikes and polymer surfaces

Giorgio De Luca [a,*], Francesco Petrosino [b], Javier Luque Di Salvo [c], Sudip Chakraborty [b], Stefano Curcio [b,*]

[a] Institute on Membrane Technology, ITM-CNR, Ponte P. Bucci, Arcavacata, 87036 Rende (CS), Cosenza, Italy
[b] Department of Computer Engineering, Modeling, Electronics and Systems (D.I.M.E.S.), University of Calabria, Via- P. Bucci, Cubo-42A, 87036 Rende (CS), Italy
[c] Dipartimento di Ingegneria (DI), Università degli Studi di Palermo– viale delle Scienze Ed.6, 90128 Palermo (PA), Italy

ARTICLE INFO

Keywords:
Long-range interaction potential energies
SARS-CoV-2 spike proteins
Closed and open structures
Molecular Mechanics and Dynamics simulations
Density Functional calculations
Surface affinity descriptors

ABSTRACT

The recent pandemic triggered numerous societal efforts aimed to control and limit the spread of SARS-CoV-2. One of these aspects is related on how the virion interacts with inanimate surfaces, which might be the source of secondary infection. Although recent works address the adsorption of the spike protein on surfaces, there is no information concerning the long-range interactions between spike and surfaces, experimented by the virion when is dispersed in the droplet before its possible adsorption. Some descriptors, namely the interaction potentials per single protein and global potentials, were calculated in this work. These descriptors, evaluated for the closed and open states of the spike protein, are correlated to the long-range noncovalent interactions between the SARS-CoV-2 spikes and polymeric surfaces. They are associated with the surface's affinity towards SARS-CoV-2 dispersed in respiratory droplets or water solutions. Molecular-Dynamics simulations were performed to model the surface of three synthetic polymeric materials: Polypropylene (PP), Polyethylene Terephthalate (PET), and Polylactic Acid (PLA), used in Molecular Mechanics simulations to define the above potentials. The descriptors show a similar trend for the three surfaces, highlighting a greater affinity towards the spikes of PP and PLA over PET. For closed and open structures, the long-range interactions with the surfaces decreased in the following order PP ~ PLA > PET and PLA > PP > PET, respectively. Thus, PLA and PP interact with the virion quite distant from these surfaces to a greater extent concerning the PET surface, however, the differences among the considered surfaces were small. The global potentials show that the long-range interactions are weak compared to classic binding energy of covalent or ionic bonds. The proposed descriptors are useful most of all for a comparative study aimed at quickly preliminary screening of polymeric surfaces. The obtained results should be validated by more accurate method which will be subject of a subsequent work.

1. Introduction

Given the significance of the surface contamination in the spread of SARS-CoV-2, attention should be paid to the design of polymeric surfaces and to the development of equipment that minimizes virus survival [1,2]. Many technological challenges need a deep understanding of the interactions between the SARS-CoV-2 and the polymeric surfaces [3,4]. A precise knowledge of such long-range interactions is fundamental since it represents an initial step for a more general comprehension of the complex phenomena occurring when infectious microdroplets are deposited on surfaces. The interaction between protein and synthetic surfaces is a noteworthy research field. A considerable amount of works analyzed this problem from different experimental perspectives and exploiting various theoretical-computational approaches [5–10]. Moreover, the study of noncovalent interactions between virus and synthetic surfaces provides useful information for materials design, in the preparation of membranes or, more generally, in the rational desing of separation devices aimed at rejecting the SARS-CoV-2.

The adsorption of coronavirus on synthetic surfaces is a highly complex phenomenon that requires a detailed description of various aspects related to different scales. The phenomenon is even more complex if natural or biological surfaces are considered for which virus-surface interaction is mediated by complex mechanisms not yet understood in detail. For this reason, it is essential to emphasize that this work

* Corresponding authors.
E-mail addresses: g.deluca@itm.cnr.it (G. De Luca), stefano.curcio@unical.it (S. Curcio).

https://doi.org/10.1016/j.seppur.2021.120125
Received 21 May 2021; Received in revised form 23 October 2021; Accepted 8 November 2021
Available online 11 November 2021

is not intended to model the adsorption of SARS-CoV-2 coronavirus and the correlated thermodynamic quantities but to provide versatile descriptors associated to long-range noncovalent interactions experimented by SARS-CoV-2 on synthetic polymeric surface showing dense and flat morphologies.

The role of respiratory droplets in the diffusion of SARS-CoV-2 has been already documented in several papers [11–13]. It is well known that the virus spreads and survives in droplets produced during coughing, sneezing, and speaking. Infectious droplets with a diameter of 125 μm–270 μm fall on surfaces [14], becoming a possible source of secondary infection. Long survival time on different surfaces was reported in the literature; overall, for glass, the virus survives over two days. For plastic, it is present over four days, although the virus concentration considered in these studies is larger than the titer realistically expected. Nevertheless, the drying time of typical respiratory droplets is on the order of minutes. In contrast, the SARS-CoV-2′s survival time on synthetic surfaces is on the order of several hours [14,15]. Bhardwaj et Agrawal showed that the coronavirus's long survival time on a surface is due to the slow evaporation of a thin nanometer liquid film remaining after the evaporation of the micro respiratory droplets. They suggested that the drying time of this nanometric film is on the order of hours, consistent with the SARS-CoV-2′s survival time. The evaporation of a large droplet volume occurs in a few minutes, whereas the evaporation of the remaining nanofilm volume is longer; thus, the viruses can survive. The coronavirus concentration is essential to determine the droplets infectivity, and it is related to the volumetric size of the droplets. Although the initial volume of the infected droplets is substantially more significant than the nanometric droplets, these latter are large enough compared to the size of the SARS-CoV-2; thus, they provide enough medium for the virus's extended survival [14]. Many researchers have assessed the decay rates of viruses' aerosol sprayed onto polymeric surfaces and onto cotton tissue, cardboard, or different materials used for protecting gears [16]. Recently, Xie et al. [17] reported measurements of an Atomic Force Microscopy (AFM) tip functionalized with spike proteins, imbided in water, and deposited over different surfaces. The experimental data shows an exponential decrease of the adhesion force with increasing protein-surface distance for all considered surfaces: metallic, glass and polymer (see Fig. 4 of reference [17]).

Considering the volume of micro and nanodroplets and the prolonged survival of the virus, the model adopted in this work assumes that the virus interacts with the surface through long-range interactions of a certain number of spike proteins due to the spherical architecture of the virion. In addition, at room temperature, immediate impacts on dense and flat surfaces do not cause stable relaxations or changes in the spike proteins' conformation (S-proteins) and surfaces, as well as the S-protein is assumed to maintain its mechanical integrity [18]. The SARS-CoV-2 is considered immersed in the potential energy field generated by the long-range noncovalent interactions of the surface; it bounces on the surface before any specific protein adsorption takes places. In particular, the range of distances considered in the work are illustrated in Scheme 1, allowing a water layer between protein and surface, i.e., the protein is not in directly contact with the surface as studied in other works [9,10]. Thus, the experimented interactions can be considered good descriptors correlated to the affinity of a given polymeric surface towards SARS-CoV-2, and *useful for a comparative study aimed at preliminary screening of polymeric surfaces*.

The virion repelled from a surface with a repulsive potential energy profile will probably be located far from the surface and it will be dispersed in the infectious droplets. Thus, in totally repelling surfaces, the surface's effect will be absent and the deposited droplets' viral environment does not change significantly concerning the initial aerosol respiratory ones. In contrast, surfaces showing high interaction with the virion, i.e., a strong attractive potential energy profile, attract the virion. As a result, depending on the surface's chemical nature, physical and chemical-adsorption processes could be triggered. Hence, when the proposed descriptors suggest marked interaction between the S-proteins and the target surface, further investigation is needed to understand if the long-range noncovalent interactions are the first step for a most stable protein absorption. Instead, an alarm should be activated when the indicators show repulsion or shallow interaction. It is important to note that the surface's noncovalent interactions do not affect hydrodynamics or buoyancy forces which are considered equal for each surface investigated in this study.

A no less negligible aspect that concerns the usefulness of proposed descriptors is screening materials for SARS-CoV-2 purification (separation), that can be used in filters or membranes. In this case, surfaces of nanopores or beads (pellets) that interact significantly with the coronavirus (i.e., showing firm attractive potential energy profiles) retain the virion while the bulk solution flows through the purification equipment; purification of SARS-CoV-2 solutions can be achieved by de-and adsorption proces.

Overall, the potential energy fields can be considered valuable descriptors for a rapid screening of synthetic surfaces [19] since they are related to the surface affinity towards SARS-CoV-2 spike; *it is worth*

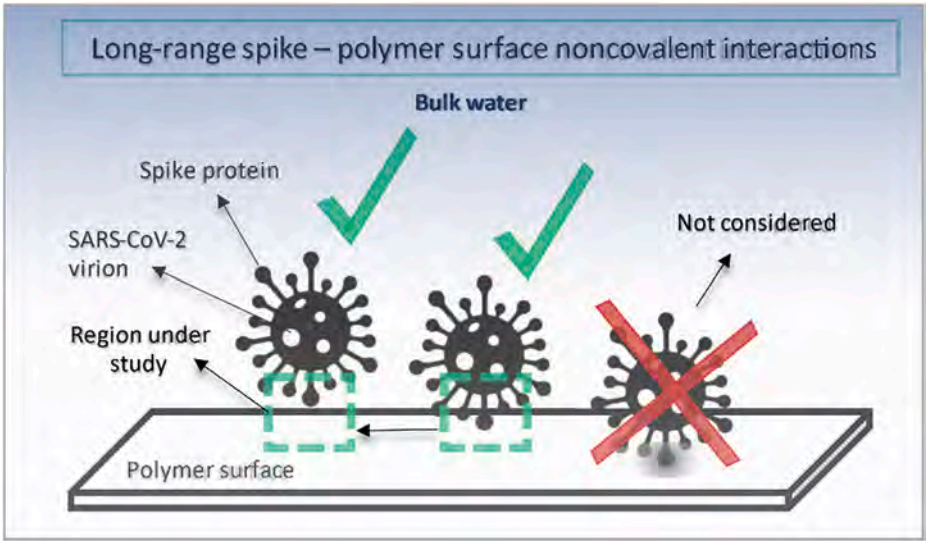

Scheme 1. Schematic representation of the long-range spike protein – polymer surface distances considered in the study, before any specific protein adsorption takes place.

noting that the descriptors do not provide thermodynamic quantity related to the virus adsorption or modifications.

To test the suggested descriptors, a comparison among three everyday polymeric synthetic surfaces was performed. The structures of the different polymers, namely polypropylene (PP), poly(ethylene) terephthalate (PET), widely used to realize personal protective equipment, as well as Polylactic Acid (PLA), were considered in the present study to evaluate by means of a multiscale computational approach the interactions between the SARS-CoV-2 spike proteins and the target materials. No study has been yet published about the combined use of *ab initio*, molecular dynamics and molecular mechanics methods to assess the aforementioned interactions.

In the framework of this modeling, the structures of the SARS-CoV-2 spikes, taken from protein databases, are used as input to evaluate the suggested descriptors; thus, protein structures containing mutations can also be used to quickly assess the surfaces' affinity towards new forms of

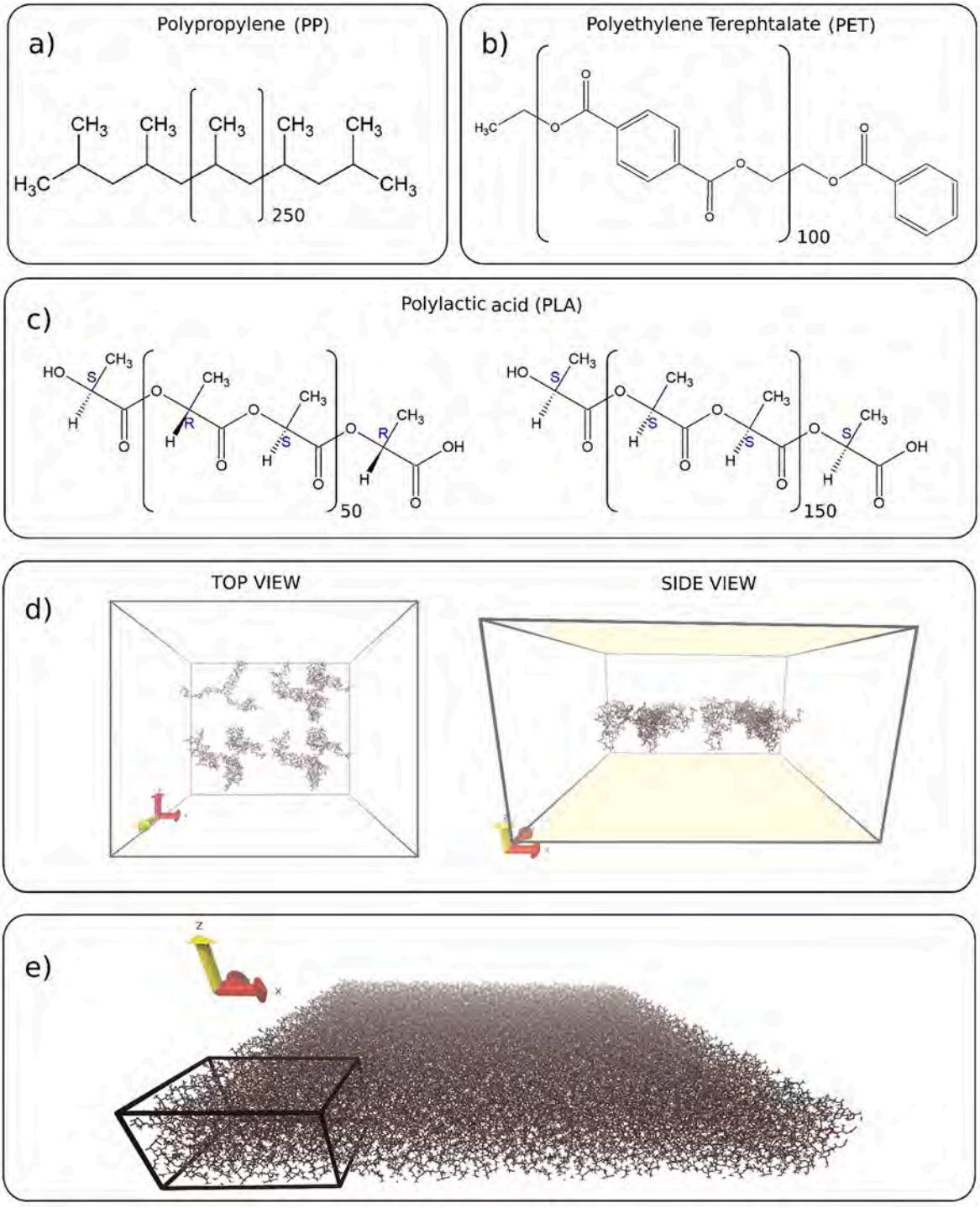

Fig. 1. Structures used in the molecular mechanics' conformational search for (**a**) Polypropylene (PP), (**b**) Polyethylene Terephthalate (PET), and (**c**) Polylactic Acid (PLA). Monomer units, extracted from the obtained lowest energy conformer, and the polymerization degree shown in brackets. (**d**) Initial configuration of PLA, showing the 2D periodic boundary conditions along xy and Lennard-Jones walls on ±z directions in yellow. **(e)** equilibrated flat PLA polymer surface with unit cell shown in black. (For interpretation of the references to colour in this figure legend, the reader is referred to the web version of this article.)

spike.

2. Computational details and models

2.1. Surface and Spike protein models

A bottom-up method was adopted to build the polymeric surfaces as successfully applied in a previous study [20]. First, a systematic conformational search based on the Molecular Mechanics approach was applied to the oligomers of the polymer surfaces (i.e., extended monomers). Then, the monomer units of PP and PE, shown in Fig. 1a and 1b, and the dimer units of PLA in stereoisomer forms (S, S) and (R, S) reported in Fig. 1c, were assembled into linear polymer chains [21], linked based on the torsional angles obtained from the previous conformational search; hence, simulated Molecular Dynamics annealing in GROMACS [22] was performed. The OPLS-AA force field [23] was used in all cases, in conjunction with the Verlet integrator with time-step 1 fs, non-bonded interactions cutoff 1 nm, PME for long-range electrostatics, and external pressure 1 atm. The surfaces models consisted of 4 chains with a degree of polymerization 250 for PP and 100 for PET, respectively, according to the average molecular weight of textile grade polymers [24], three chains of poly (L-lactic acid) (PLLA) plus one chain of poly (D, L-lactic acid) (PDLA) with degrees of polymerization 150 and 50 correspondings to 10 mol% content of D-lactic acid, as commonly used in PLA production [25]. The polymer surfaces' equilibration consisted of heating-cooling cycles in the NPT ensemble, until a stable response on density, potential energy, root mean square displacement, and radius of gyration were obtained, which was achieved after applying at least 40 heating-cooling cycles, depending on the surface. A single NPT heating-cooling cycle had a duration of 250 ps and consisted in the following: the firsts 50 ps at constant temperature (300 K), then a linear increase of the temperature of 300–450 K for 50 ps, further 50 ps at constant T (450 K), a linear temperature decrease of 450–300 K for 50 ps, and final 50 ps at constant T (300 K). After the simulated annealing, 3 ns in NPT at 300 K were applied to allow equilibration at constant temperature.

To achieve reliable surface models, 2D periodic boundary conditions in the *xy* plane were applied while Lennard-Jones (LJ) potential walls in $\pm$ z directions were imposed, slab model (Fig. 1d). Finally, the equilibrated flat surfaces were replicated in the *xy* plane (Fig. 1e) to yield larger surfaces, with a dimension of 25 $\times$ 25 nm, used in the computation of the interactions between spike protein and polymer (Section 2.2).

The equilibrated surfaces show surface topographies essentially flat as it would have been expected for polymeric surfaces at the studied dimensions, i.e., tens of nanometers. Moreover, these surfaces did not show pores, cavities, or defects higher than few angstroms, neither pending functional groups over the surface.

The S-protein is a trimeric unit formed by three polypeptide chains of identical primary structure (chains A, B, and C). It is divided into two subunits: the S1 (residues 1-1146 per chain) is the utmost subunit, i.e., the head of the protein with a clove shape exposed to the exterior of virus and hence mainly responsible for the contact with the polymer surface, whereas the subunit S2 (residues 1146-1273 per chain) is the transmembrane tail that links the S-protein to virion through the bi-lipid membrane. To study the interaction of the SARS-CoV-2 spikes with the target surfaces, the complete structure of the S1 subunit was downloaded. Two different configurations were considered as shown in Fig. 2: the closed state (PDB code: 6VXX), in which the three polypeptide chains cover the Receptor Binding Domain (RBD), and an open prefusion state (PDB code: 6VSB), in which one polypeptide chain is lifted to expose the RBD [26]. The crystal structures of both configurations were taken from the SARS-CoV-2 protein library of the CHARMM-GUI suite (Fully-glycosylated S protein head-only models, codes 6VXX and 6VSB) [27]). The downloaded systems are based on the cryo-EM resolved crystal structures, reported a few weeks after the pandemic outbreak by Walls et al. [26], plus the predicted missing residues and the binding glycans reported by Woo et al. [27].

Spike proteins are surrounded by an essential number of binding polysaccharides [26,28] that affect their interactions with the polymer surfaces. Their atomic partial charges were determined via quantum calculations based on Density Functional Theory performed on the glycan structures identified on the subunit S1 [27]. Fig. 3 shows two illustrative examples of such polysaccharide structures; for a complete list of glycans, protein binding sites, and further details, see reference [27]. The quantum calculations for the partial charges evaluation were carried out using the B3LYP exchange-correlation functional considering dispersion correction through Grimme's DFT-D3 approach [29]. The energy convergence in the self-consistent cycles and the density matrix threshold were set to 1.0×10^{-6} a.u. and 2.0×10^{-6} a.u., respectively. Gaussian type double-ζ 6-31G plus polarization function basis set on N, C, and O atoms was used. DFT calculations were performed on the NWChem package [30].

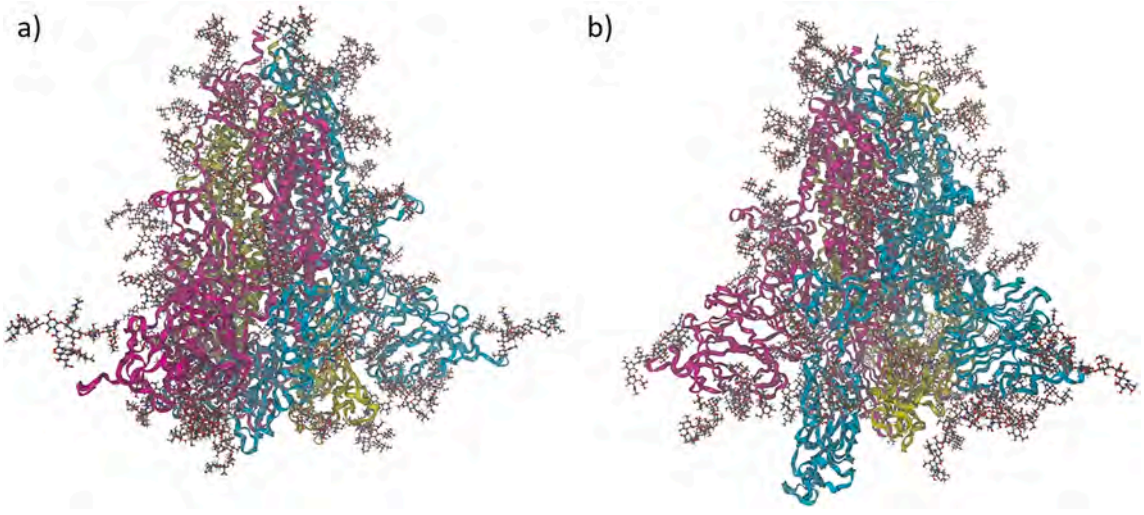

Fig. 2. S-protein subdomains S1 used in the modeling, showing the polypeptide chain A (cyan), chain B (magenta), and chain C (yellow) in ribbon representation and binding glycans in ball-stick representation. (**a**) Closed configuration (PDB code 6VXX [26,27]) and (**b**) Open configuration with chain A lifted (PDB code 6VSB [26,27]). (For interpretation of the references to colour in this figure legend, the reader is referred to the web version of this article.)

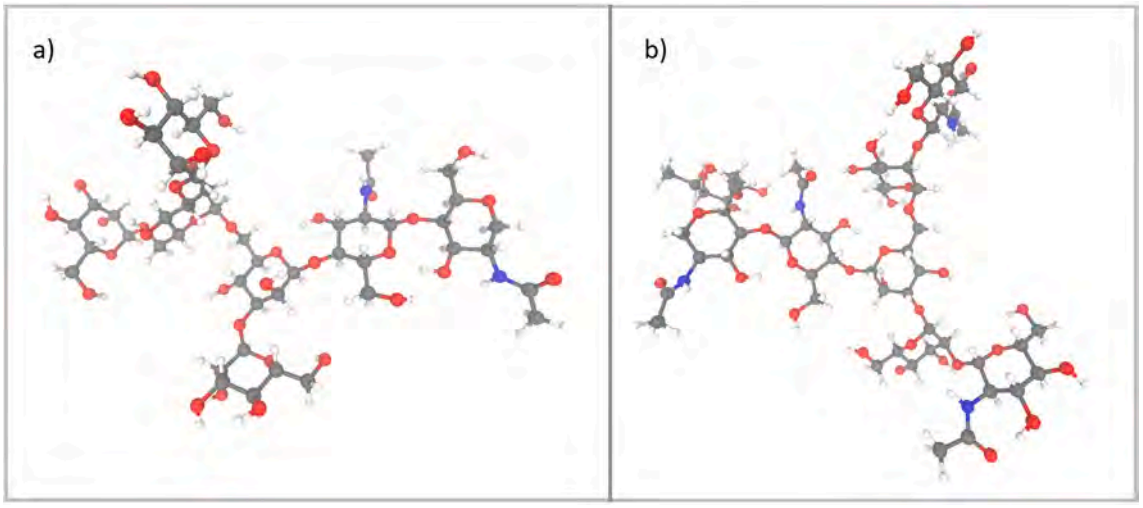

Fig. 3. Structures of some N-glycans that bind to the Spike proteins used in the single-point DFT calculations for the atomic partial charge assignment. (**a**) N-Glycan composed of 5 mannoses and 2 N-acetylgalactosamines, identified on 7 of the 19 binding sites per polypeptide chain, (**b**) N-Glycan composed of 3 mannoses, 4 N-acetylgalactosamines, and 1 fucose, identified on 5 of the 19 binding sites per polypeptide chain. Carbon atoms in grey, oxygen atoms in red, nitrogen atoms in blue, hydrogen atoms in white. (For interpretation of the references to colour in this figure legend, the reader is referred to the web version of this article.)

2.2. Interaction potential energies

The noncovalent interactions between the single S-protein and the target surfaces, as well as the global interaction potentials, were calculated using a classic Molecular Mechanics approach.

In particular, the single-protein potential describes the potential energy of a single spike interacting with the polymer surface; thus, the surrounding protein's effects are not considered. The second potential is instead the interaction potential due to a protein ensemble formed by a reference spike, considered perpendicular to polymer surface, and its surrounding proteins: i.e., the 1st and 2nd neighbors. Hence, both descriptors are correlated with the affinity of SARS-CoV-2 towards a target polymer surface.

2.2.1. Single-protein interaction potentials

Based on the work of the Lund and Jönsson [31] and our previous works [32–34], single-protein interaction potentials, U_{sp}, were defined as the sum of three main contributions:

$$U_{sp} = U_{hs} + U_{el} + U_{vdW} \tag{1}$$

where

$$U_{hs} = \begin{cases} \infty & r_{ij} < \dfrac{\sigma_{ii} + \sigma_{jj}}{2} \\ 0 & r_{ij} > \dfrac{\sigma_{ii} + \sigma_{jj}}{2} \end{cases} \tag{2}$$

$$U_{el} = \sum_i \sum_j \frac{q_i q_j}{4\pi\epsilon_0 \epsilon_r r_{ij}} \tag{3}$$

$$U_{vdW} = \sum_i \sum_j 4\epsilon_{ij} \left[\left(\frac{\sigma_{ij}}{r_{ij}} \right)^{12} - \left(\frac{\sigma_{ij}}{r_{ij}} \right)^{6} \right] \tag{4}$$

Specifically, U_{hs} considers the repulsion of electron clouds through a hard-spheres model for each atoms pair of the protein-surface system. U_{el} is the total Coulomb interaction defined by the atomic charges, q_i, and q_j, of the spike protein, glycans and polymer surface, while a Lennard-Jones 12-6 potential was used to evaluate the hydrophobic interactions, i.e., the van der Waals contribution U_{vdW}. Partial charges and Lennard-Jones parameters for protein and polymers were taken from the Amber [35] and the OPLS [23] force-fields, respectively, while, the glycans van der Waals parameters were taken from the GLYCAM library [36]. The atomic partial charges of bonded glycans over the protein surface, were determined through DFT based calculations. ε_0 and ε_r are the *vacuum* and the relative water permittivity, the latter was fixed equal to 78.2, respectively. To avoid errors due to the cutoff in the evaluation of the U_{el} and U_{vdW} contributions, all the atoms of the protein, glycans and polymer surface were considered in the sums in Eqs. (3) and (4). This results in a significant computational effort, and it represents to our knowledge the first attempt at such extensive molecular mechanics simulations on these systems.

The r_{ij} distance that defines the U_{sp} contributions is the distance between the *i-th* atom of the protein (or binding glycans) and the *j-th* atom of the polymer surface. Each r_{ij} was written as a function of the distance between the geometric centers of the surface and of the spike lying along the *z*-axis perpendicular to the surface, i.e, the distance $d = d_o + n\Delta s$; d was elongated by $n\Delta s$ steps, starting from d_0^C or d_0^O (see Fig. 4a, b, and e), until 130 Å with Δs equal to 5 Å. As a result, U_{sp} becomes a function of the center-to-center distance d, $U_{sp}(d)$. It is important to point out that once defined d as input, each r_{ij} distance is calculated to obtain the different contributions, hence an all-atom description of protein-polymer surface was adopted yielding roughly more than 10^5 atoms per system. A bespoke [33] code was implemented throughout a set of MATLAB functions to calculate $U_{sp}(d)$, according to Eqs. (1)–(4).

The initial distances d_0^C and d_0^O were chosen to avoid any overlapping between the atoms of the S-proteins and polymer surfaces as well as considering a minimum number of water molecules between the interacting systems. It is important to emphasize that the starting distances depend on the spike structures and orientations on the polymer surface, as shown in Fig. 4. For the closed spike in perpendicular orientation, the starting distance, d_0^C, is 80 Å (Fig. 4a), while for the open structure d_0^O results in 90 Å (Fig. 4e). In particular, the starting distance changes according to the different clove forms of the closed and open states as well as to the adsorbed polysaccharides. It is important to emphasize that the present modeling takes this important aspect into account.

For each set of calculations, the d distance ranges from the above starting distances (d_0^C and d_0^O) to 130 Å, considering a lower limit of 72 Å for the closed spike, corresponding to the closest structure where the protein approached the surface into a "no-gap" configuration, i.e., without water molecules between the interacting systems. It is worth noting that no calculations at "no-gap" configurations were carried out because, as reported also below, the dielectric permittivity for the water

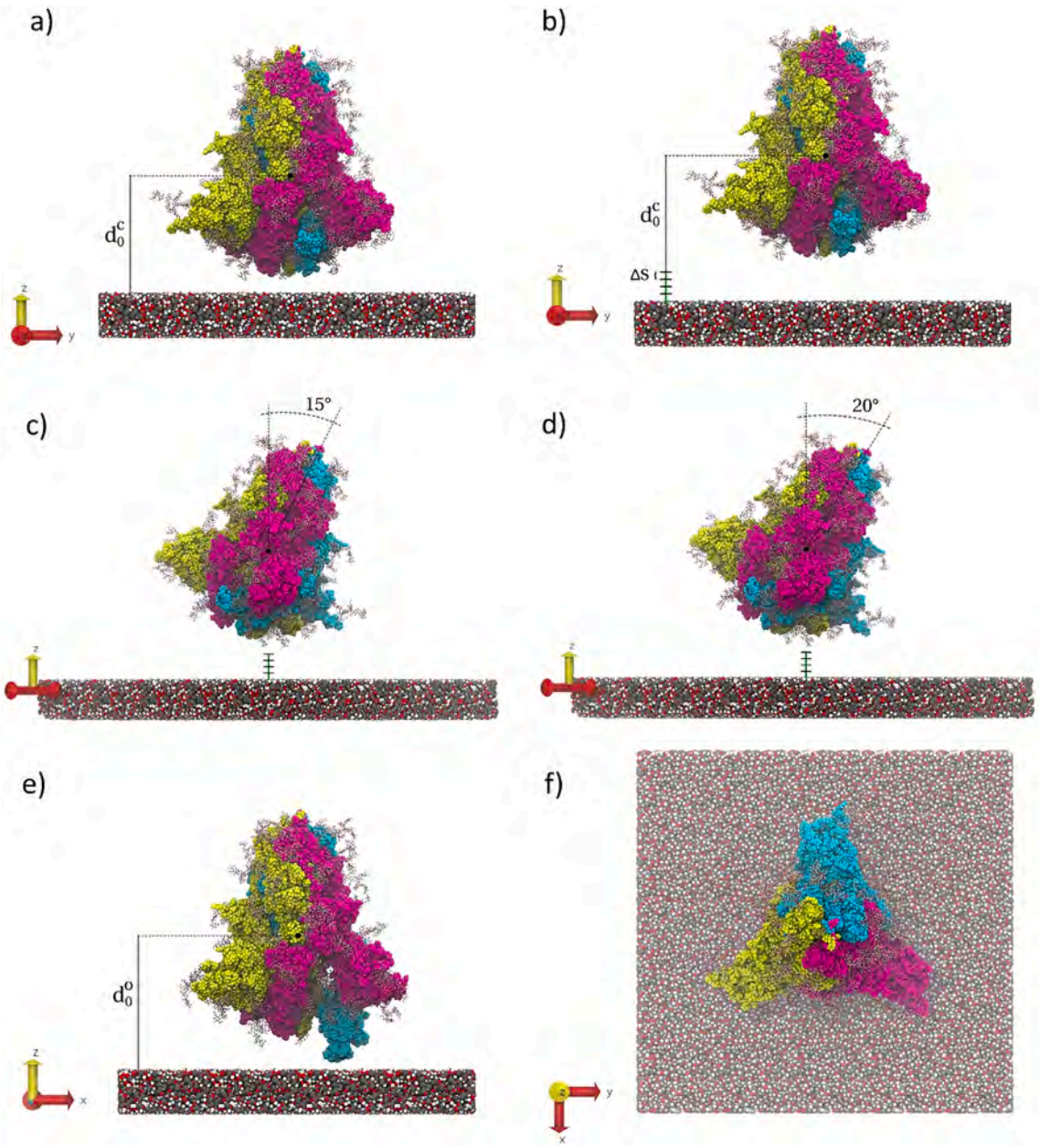

Fig. 4. (**a**) Spike protein in the closed state on PLA surface in perpendicular orientation at $d_0^C = 80$ Å, defined as the distance between the geometrical centers of the protein and polymer surface. (**b**) Spike protein in a closed state at a distance from polymer surface of 100 Å, obtained by pulling four steps $\Delta s = 5$ Å along the *z* axis. (**c**) Closed S-protein tilted 15° towards one of the corners of the polymer surface. (**d**) Closed S-protein tilted 20° towards one of the corners of the polymer surface. (**e**) Spike protein in an open state on top of the polymer surface at a distance $d_0^O = 90$ Å (**f**) Top view of a Spike protein above the PLA surface. Atoms of the Spike polypeptide chain A (cyan), chain B (magenta), and chain C (yellow) are shown as spheres, atoms of glycans are shown in ball and stick representations, and atoms of the PLA surface are shown as van der Waals spheres, carbon atoms in grey, oxygen atoms in red, hydrogen atoms in white and nitrogen atoms in blue. (For interpretation of the references to colour in this figure legend, the reader is referred to the web version of this article.)

very near the surface is different from the used bulk water value. The *d* distances were calculated for various protein orientations defined through the tilt angle (θ), shown in Fig. 4c hence, each r_{ij}distances were calculated from the spike-surface *xyz* coordinates subtracted van der Waals radius of corresponding atomic (σ_{ii}). Consequently, the bespoke algorithm avoids possible overlapping between protein or glycans atoms and those of the polymer.

Due to the virus spherical surface, the S-protein assumes different orientations with regard to a spike perpendicular to the polymer surface, thus the single-protein interaction potentials, $U_{sp}(d)$, were evaluated for different tilt angles, θ_i, to define the global potentials. A model based on geometrical considerations was then used to find the inclinations of the proteins closest to the reference spike; the details of this geometrical model were reported in Support Information. Using the values reported in Table S1, three different orientations were considered in the calculations of the $U_{sp}(d)$ potentials, respectively equal to $\theta = 0°$ (perpendicular), $\theta = 15°$ and $\theta = 20°$; the angles shown in Table S1 were approximated to integer for an easier displacement of the protein respect to the polymer surfaces. The Δd_i values, reported in Tables S1 and corresponding to the increment that must be added to the center-to-center distance of the perpendicular protein, were used for the calculation of the single-protein potentials of the inclined spikes. It is worth noting that the sum of Δd_i to the center-to-center distance, used to evaluate the distance of the inclined proteins from the surface, is valid

only for not large inclinations. Considering the unit cell, used to describe the distribution of the spikes on the virion membrane around the reference protein (see Support Information for details), the single-protein potentials were calculated using four main orientations associated with the following combinations of the tilt angles pairs: θ_x/θ_y = 15°/15°, 15°/−15°, −15°/15°, −15°/−15° and similarly for the θ = 20°. The potential $U_{sp}(d)$ was then evaluated for each of these combinations to obtain average single-protein interaction potentials: $U_{sp,av,15^\circ}(d)$ and $U_{sp,av,20^\circ}(d)$ for θ = 15° and θ = 20°, respectively. For the S-protein perpendicular to the polimeric surface the $U_{sp,per}(d)$ result just equal to the sum of Eqs. (1)–(4) where all r_{ij} distances are evaluated from the spike-surface *xyz* coordinates associated to a fixed center-to-center *d* distance. The average potentials and $U_{sp,per}(d)$ were hence used to evaluate the global interaction potentials as illustrated in the next

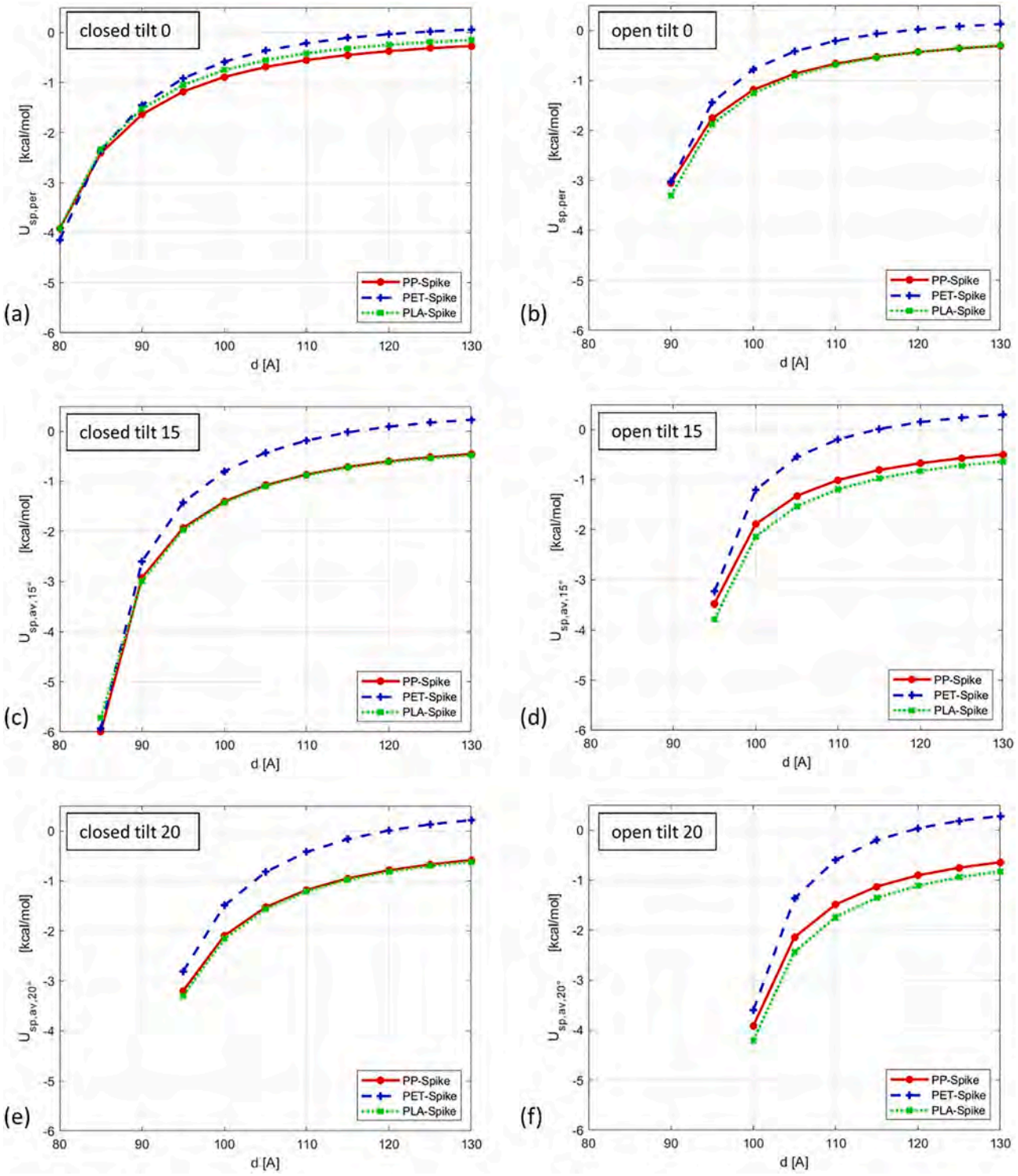

Fig. 5. Single-protein interaction potentials as a function of the protein-surface distance (*d*) for the target surfaces. a) potential energies for the closed and b) open S-protein structures in perpendicular orientation. c) average potentials for closed and d) open S-protein structures inclined concerning polymer surface of 15°. e) average potentials for closed and f) open S-protein structures inclined concerning polymer surface of 20°.

section.

2.2.2. Global interaction potentials

To calculate the global potentials, we assumed that each spike around the central S-protein, perpendicular to the polymeric surface, contributes to the global interaction potentials according to its inclination, associated to the angle θ_i, and considering a protein-surface distance obtained summing Δd_i increments to the center-to-center distance of the protein in the perperticular orientation. Thus, the global potential field was defined as:

$$U_{Glo}(d) = U_{sp,per}(d) + n \cdot U_{sp,av,15^\circ}(d + \Delta d_i) + m \cdot U_{sp,av,20^\circ}(d + \Delta d_{4,4'}) \quad (5)$$

where $U_{sp,per}(d)$ is the single-protein potential of the perpendicular spike located at d distance, n is the number of the neighbors proteins showing tilt angles near 15° and $U_{sp,av,15^\circ}(d+\Delta d_i)$ is the average single-protein

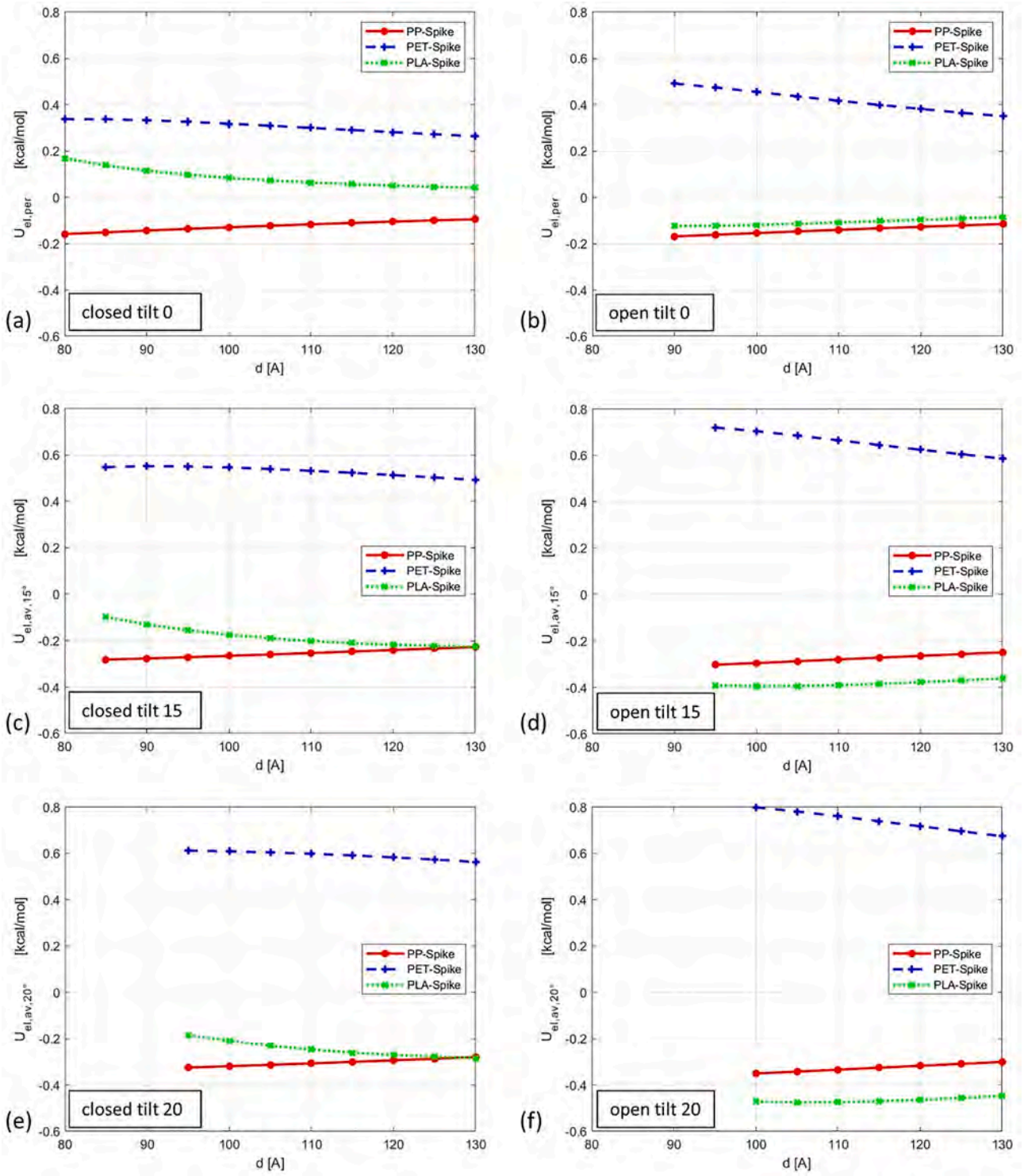

Fig. 6. Electrostatic contributions to the single-protein interaction potentials as a function of d distance for the target surfaces. a) $U_{el,per}(d)$ for closed and b) open spike structures in perpendicular orientation. c) Average $U_{el,av,15^\circ}(d)$ for closed and b) open spike structures inclined concerning the surface of 15°. e) Average $U_{el,av,20^\circ}(d)$ for closed and b) open spike structures inclined inclined concerning the surface of 20°.

potential evaluated at $d + \Delta d_i$(for i index see Fig. S1 and Table S1 in Support Information), m is the number of spike proteins corresponding to the 2nd neighbors that show tilt angles approximately of 20° while $U_{sp,av,20^\circ}$ is the average single-protein potential evaluated at a distance equal to $d + \Delta d_{4,4'}$.

3. Result and discussion

The single-protein potentials: $U_{sp,per}(d)$, $U_{sp,av,15^\circ}(d)$ and $U_{sp,av,20^\circ}(d)$ as a function of the spike-surface distance, d, for the open and closed structures were shown in Fig. 5.

The figure's analysis shows that the PET-spike potentials are appreciably different from those associated with PP and PLA surfaces;

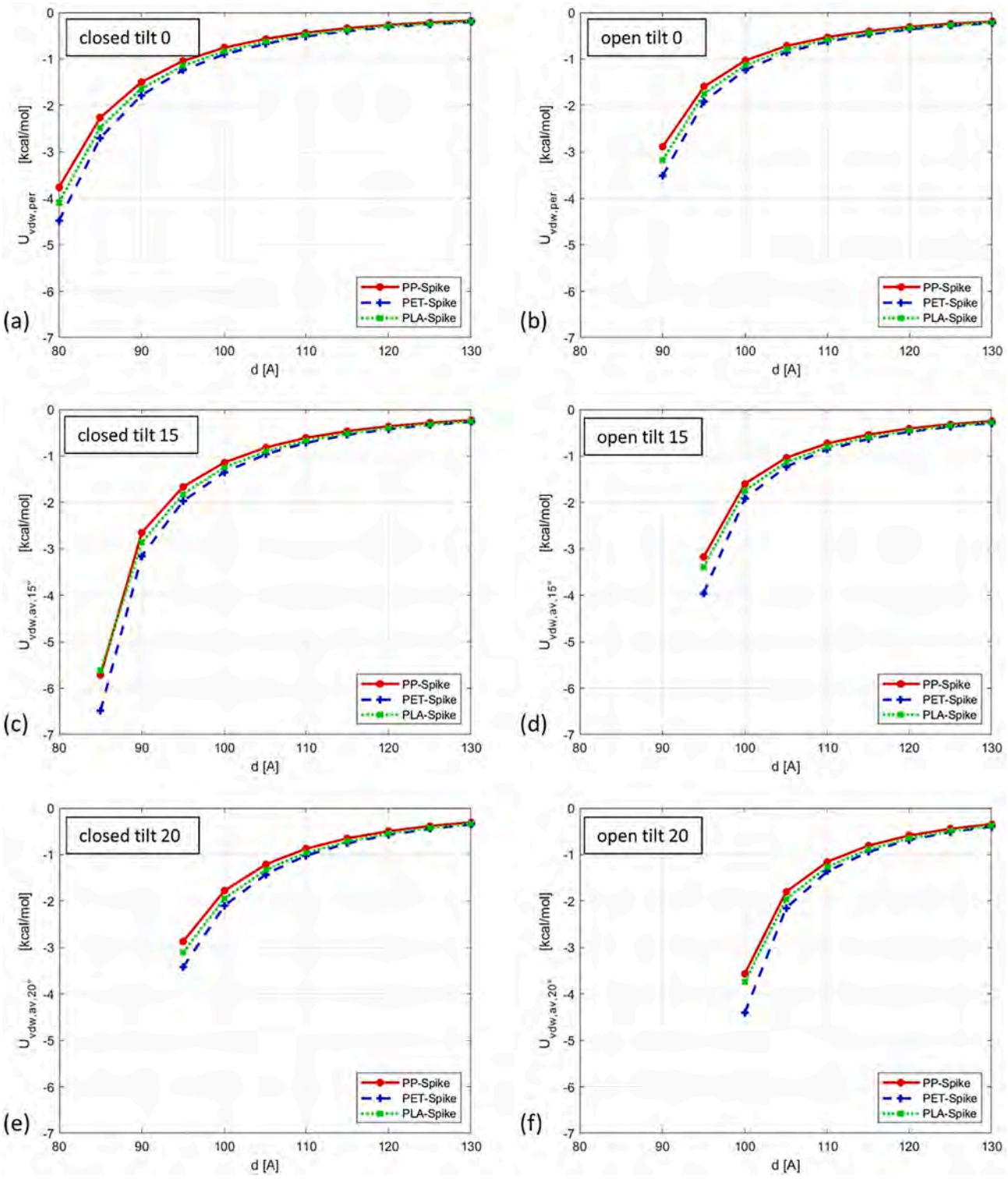

Fig. 7. Hydrophobic contributions to the single-protein interaction potentials as a function of d distance for the target surfaces. a) $U_{vdW,per}(d)$ for closed and b) open spike structures in perpendicular orientation. c) Average $U_{vdW,av,15^\circ}(d)$ for closed and b) open spike structures inclined concerning the surface of 15°. e) Average $U_{vdW,av,20^\circ}(d)$ for closed and b) open spike structures inclined inclined concerning the surface of 20°.

this difference results less pronounced for the closed structure in perpendicular orientation. The differences among the single-protein potentials are more marked for high protein-surface distances, whereas near the surfaces, they are reduced or cancel out, as shown in Fig. 5a, b, c. Overall, the descriptors indicate that the closed and open spike protein interacts with the PET surface to a lesser extent concerning the other surfaces.

To better understand the reason for this trend, the electrostatic and van der Waals average contributions, $U_{el,av}(d)$ and $U_{vdW,av}(d)$, as well as the corresponding contributions referred to as the perpendicular spike, were shown in Fig. 6 and Fig. 7, respectively. Herein, we correlate U_{el} and U_{vdW} to hydrophilic and hydrophobic contributions, respectively. The electrostatic contributions show a similar behavior of total potentials: $U_{sp,per}(d)$, $U_{sp,av,15^\circ}(d)$ and $U_{sp,av,20^\circ}(d)$ (Fig. 5). Conversely, the hydrophobic contributions show an opposite trend concerning the total single-protein potentials, that is the spike-surface interactions decrease in the order PET > PLA > PP. However, since the differences among the $U_{vdW}(d)$ are small, then the electrostatic contributions can reverse the trend so that the interactions between the PET surface and the single spike results to a lesser extent concerning the other surfaces as previously found for the $U_{sp,per}(d)$, $U_{sp,av,15^\circ}(d)$ and $U_{sp,av,20^\circ}(d)$ potentials.

This means that the electrostatic contribution, albeit small, is the driving force determining the behavior of the single-protein interaction potentials both for open and closed structures. The comparison between the electrostatic and hydrophobic contributions also highlights that for each considered surface and protein state, $U_{vdW}(d)$ is negative that corresponds to attractive potential whereas $U_{el}(d)$ is positive for PET, corresponding to a repulsive potential, and slightly negative for PP and PLA surfaces. In addition, the hydrophilic interaction is markedly smaller than the hydrophobic one; hence, this result evidences that the SARS-CoV-2 spike interacts with the considered surfaces mainly through the hydrophobic interactions. It is interesting to note that, in Fig. 6 of reference [17], the main non-covalent interactions between the spike-functionalized AFM tip and the polymeric surfaces are mostly hydrophobic; thus, our result is in qualitative agreement with experimental data of ref. [17]. To explain this finding, the S-protein showing hydrophilic and hydrophobic residues was shown in *Support Information*.

Since the electrostatic contributions determine the PLA > PP > PET trend of the single-protein interaction potentials, particular attention must be paid to the water dielectric permittivity's value near the target surfaces. For distances below 5 – 10 Å, the water dielectric permittivity is different from the value of bulk water [37] due to confinement effects; thus, in this range, the electrostatic contribution might not be fully reliable. However, for larger distances as illustrated in Scheme 1, the bulk value of the permittivity is a reasonable assumption.

To test the dielectric permittivity effect on the single-protein interaction potentials, calculations with a dielectric constant of 40 were also carried out. The obtained results are not appreciable different from those reported.

As shown in Fig. 5, the differences among the single-protein potentials are not too large, however, it is important to reiterate that the above potentials refer to the interaction of just one protein; thus, these differences will become more marked if various proteins are considered in the calculation of the potentials, i.e, considering the global interaction potentials.

In order to evaluate the contribution of various spikes around a reference protein, i.e., the effect of the 1st and $^{n}2^{nd}$ neighbors, the global interaction potentials were evaluated according to equation (5), exploiting the single-protein potentials ($U_{sp,per}(d)$, $U_{sp,av,15^\circ}(d)$ and $U_{sp,av,20^\circ}(d)$), and plotted in Fig. 8. Since the global potential is the sum of individual potentials, the overall trend does not change. However, the differences between the global PET-spike potentials and those associated with PP and PLA surfaces became more evident.

According to these potentials (Fig. 8), again, PP and PLA surfaces interact with the S-proteins to a greater extent than the PET surface. Additionally, the global potentials highlight more clearly that the PP and PLA surfaces interact differently with the open state of the S-protein (Fig. 8 b), whereas, these surfaces display equal interaction with the closed state (Fig. 8a). This result could be exploited to distinguish two different spike configurations. In particular, Fig. 4 of reference [17] (adhesion force-distance profile), shows an exponential decrease of the adhesion force with increasing protein-surface distance. Although it is difficult to extract accurate experimental values of the spike-polymer adhesion force at very short distances (below 2.5 nm), for distances above 2.5 nm, we can observe very low adhesion force. This experimental behaviour is in qualitative agreement with our interaction energy profile for protein-surface distances above 1 nm, as it can be seen in Fig. 8.

The protein-surface interactions are weak compared to classic binding energy of covalent or ionic bonds, and the global potentials of Fig. 8 indicate that the first step of a possible adhesion of the virion on the surfaces is not triggered by molecular electrostatic and hydrophobic forces, but rather from mesoscale and macroscale interactions whose calculations are beyond the scope of this work. At the mesoscale a larger system should be considered and the calculated microscopic interactions will be the basis for the mesoscale simulations of a system composed of multiple virion particles interacting with the surface, in which the single protein is considered by a coarsed model. In this case, it will be

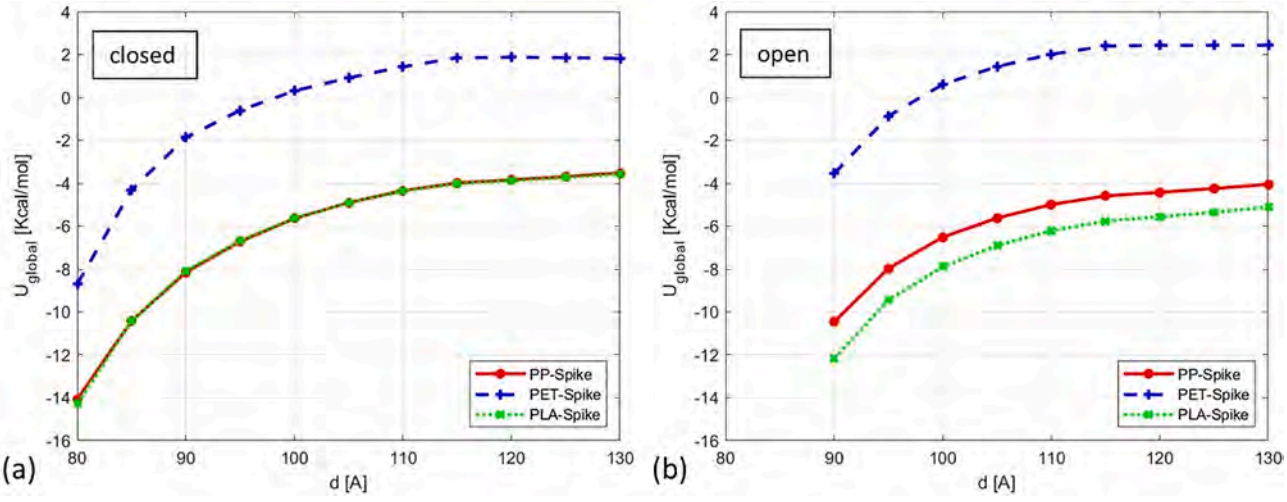

Fig. 8. a) Global interaction potentials as a function of the protein-surface distance (d) for the closed structure of spike and target surfaces, b) global interaction potentials as a function of the protein-surface distance (d) for the open structure of spike.

convenient to use stochastic approaches such as Monte Carlo methods for the calculation of global potentials starting anyway from the interaction models already used in this work [38]. A quantification of such a molecular long-range interactions, *via* the single-point calculations performed, is useful and informative in such a complex scenario. In addition, some important factors can be mentioned as crucial in determining the fate of virions over polymeric surfaces. At the macroscale, the relative humidity has an effect on the water droplet evaporation-condensation rate [14,15,39]; lower the relative humidity, longer the droplet lifetime [39] and longer the virion survival probability [40]. Therefore, the possible virion deposition over the surface might be mediated by gravity, or by pressure-driven forces which control the movement of the particles (virion) inside the water droplet.

From a macroscopic point of view, the descriptors shown in Fig. 8 indicate that PP and PLA should affect the virus in respiratory droplets adsorbed on these surfaces to a greater extent concerning PET surfaces. Moreover, the global interaction potentials show that PP and PLA-based purification devices or membranes should retain the virus more effectively than PET-based devices.

Considering certain flexibility of the bi-lipidic membrane due to the pleomorphism of the virion [41,42], the global potentials were evaluated (Fig. 9) taking into account the reference spike, the 1st, and 2nd neighbors proteins at the same distance from the polymer surface; this means to consider an alignment of the proteins.

These potentials, associated with a flat spikes arrangement, show for large protein-surfaces distances a behavior similar to the previous global potentials. However, the flat global potentials' differences cancel out for the closed structure and protein-surface distance smaller than 90 Å. Unlike the previous global potentials, in this case, the PP and PLA surfaces can no longer distinguish the open structure of the spike from closed configuration. However, from a qualitative point of view, the flat global potentials provide information equal to that provided by the previous descriptors: the PET surface interacts, at long distance, with the SARS-CoV-2 spike proteins to a lesser extent than the other investigated surfaces. Although these potentials' values are markedly larger than the previous potentials, they remain in the range of weak noncovalent interactions compared to covalent or ionic bonds. Thus, they confirm that the first step of a subsequently virion's adsorption, dispersed in the droplets bulk, is not controlled by molecular electrostatic and hydrophobic long-range interactions. Such conclusion has significant implications in various fields, such as biology or materials engineering, to limit SARS-CoV-2 spreading.

A more complex model in which the reference protein and the neighboring spikes are floating, changing their orientation [43] and distance from the surface, would be more accurate. However, we believe that the descriptors associated with such a more accurate model should provide similar trends to those found using the limit cases, i.e., the rigid and completely flat arrangements, herein analyzed. The validation of this statement goes beyond the scope of this paper.

4. Conclusion

Long-range noncovalent interactions between the SARS-CoV-2 spikes and synthetic polymeric materials were investigated to suggest descriptors associated with the surface's affinity towards coronavirus. Single-protein and global interaction potentials, evaluated through a combined computational approach based on molecular mechanics and dynamics simulations, were proposed as versatile descriptors. The partial charges of the glycans deposited on the spike surface were evaluated by means of quantum mechanics calculations. Based on the spherical architecture of the viron, showing pending S-proteins, the model adopted in this work assumes that the it interacts with the surface through long-range interactions with a certain number of proteins and, at room temperature, immediate impacts on dense and flat surfaces do not cause stable relaxations or changes in the proteins and surfaces structures.

The evaluated descriptors highlight that the protein-surface long-range interactions decreases in the following order PP ~ PLA > PET and PLA > PP > PET for the closed and open structures of the spike, respectively; although the differences among the descriptors are small to draw final conclusions on the affinity of the tested surfaces towards SARS-CoV-2 spikes. The PLA and PP surfaces should affect viruses, dispersed in the droplets, to a greater extent concerning the PET surface. As a result, the descriptors suggest that PP and PLA-based purification devices (e.g. filters or membranes) should retain the virus more effectively than PET-based systems.

The values of the global potentials show that the proetein-surface long-range interactions are weak compared to classic binding energy of covalent or ionic bonds. The order of magnitude of the global potentials indicate that the first step of a subsequently adhesion of the virion on the surfaces, dispersed in the droplets bulk, is not controlled by molecular electrostatic and hydrophobic long-range interactions but rather from mesoscale and macroscale forces whose description is beyond the scope of this work. Such conclusion could have significant implications in various fields, such as biology or materials engineering, to limit SARS-CoV-2 spreading.

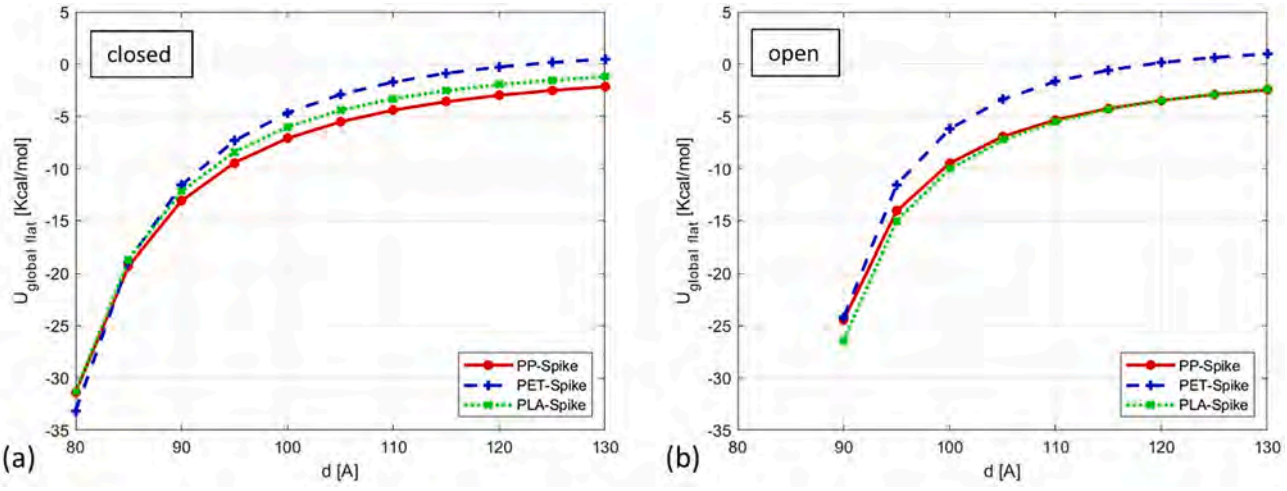

Fig. 9. a) Global interaction potentials as a function of the protein-surface distance (*d*) for the spike closed structure and target surfaces assuming specific feasibility of the virus membrane: **b)** Global interaction potentials as a function of the protein-surface distance (*d*) for the open structure and target surfaces assuming specific feasibility of the virus membrane.

The global descriptors show that two surfaces (PP, PLA) can interact differently with the open configuration of the S-protein (Fig. 8); this could be exploited to distinguish two different spike configurations. Moreover, since the proposed descriptors consider the different protein's clove forms (i.e., closed and open) as well as adsorbed polysaccharides, they could highlight surfaces affinity towards proteins with recently appeared mutations. At the moment, the analysis of the energetic contributions is based on electrostatic and van der Waals terms; nevertheless, this analysis is mainly aimed at a comparative study because the potentials of individual proteins were evaluated at long protein-surface distances following the approach of some previous studies. This analysis should be useful as a first step for future works, that might be interested in the characterization of contributions of spike-polymer interactions based on different components of the spike protein, such as binding glycans. Undeniably, the obtained qualitative results should be validated by more accurate methods, but this will be the purpose of a subsequent work.

CRediT authorship contribution statement

Giorgio De Luca: Conceptualization, Methodology, Investigation, Writing – original draft, Writing – review & editing, Data curation. **Francesco Petrosino:** Software, Visualization, Investigation, Writing – original draft, Data curation. **Javier Luque Di Salvo:** Visualization, Investigation, Data curation, Writing – original draft, Writing – review & editing. **Sudip Chakraborty:** Supervision, Validation, Writing – original draft. **Stefano Curcio:** Supervision, Validation, Project administration, Writing – original draft.

Declaration of Competing Interest

The authors declare that they have no known competing financial interests or personal relationships that could have appeared to influence the work reported in this paper.

Appendix A. Supplementary material

Supplementary data to this article can be found online at https://doi.org/10.1016/j.seppur.2021.120125.

References

[1] E. Tuladhar, W.C. Hazeleger, M. Koopmans, M.H. Zwietering, R.R. Beumer, E. Duizer, Residual Viral and Bacterial Contamination of Surfaces after Cleaning and Disinfection, Appl. Environ. Microbiol. 78 (21) (2012) 7769–7775, https://doi.org/10.1128/AEM.02144-12.

[2] P.Y. Chia, K.K. Coleman, Y.K. Tan, S. Wei, X. Ong, M. Gum, S.K. Lau, X.F. Lim, A. S. Lim, S. Sutjipto, P.H. Lee, T.T. Son, B.E. Young, D.K. Milton, G.C. Gray, S. Schuster, T. Barkham, P.P. De, S. Vasoo, M. Chan, B. Sze, P. Ang, SARS-CoV-2 in hospital rooms of infected patients, Nat. Commun. 11 (2020), https://doi.org/10.1038/s41467-020-16670-2.

[3] T. Zhao, A. Elzatahry, X. Li, D. Zhao, Single-micelle-directed synthesis of mesoporous materials, Nat. Rev. Mater. 4 (12) (2019) 775–791, https://doi.org/10.1038/s41578-019-0144-x.

[4] M.A. Kostiainen, P. Hiekkataipale, J.Á. de la Torre, R.J.M. Nolte, J.J.L. M. Cornelissen, Electrostatic self-assembly of virus – polymer complexes, J. Mater. 21 (7) (2011) 2112–2117, https://doi.org/10.1039/C0JM02592E.

[5] Y.u. Hoshino, H. Lee, Y. Miura, Interaction between synthetic particles and biomacromolecules: fundamental study of nonspecific interaction and design of nanoparticles that recognize target molecules, Polym. J. 46 (9) (2014) 537–545, https://doi.org/10.1038/pj.2014.33.

[6] R.A. Latour, Molecular simulation of protein-surface interactions: Benefits, problems, solutions, and future directions (Review), Biointerphases. 3 (3) (2008) FC2–FC12, https://doi.org/10.1116/1.2965132.

[7] X. Lu, P. Xu, H.-M. Ding, Y.-S. Yu, D.a. Huo, Y.-Q. Ma, Tailoring the component of protein corona via simple chemistry, Nat. Commun. 10 (1) (2019), https://doi.org/10.1038/s41467-019-12470-5.

[8] I. Medintz, Universal tools for biomolecular attachment to surfaces, Nat. Mater. 5 (2006) 20375, https://doi.org/10.1038/nmat1776.

[9] D.C. Malaspina, L. Pérez-fuentes, C. Drummond, D. Bastos-González, J. Faraudo, Protein-surface interactions at the nanoscale: Atomistic simulations with implicit solvent models, Curr. Opin. Colloid Interface Sci. 41 (2019) 40–49, https://doi.org/10.1016/j.cocis.2018.11.005.

[10] D.C. Malaspina, J. Faraudo, Computer simulations of the interaction between SARS-CoV-2 spike glycoprotein and different surfaces, Biointerphases. 15 (5) (2020) 051008, https://doi.org/10.1116/6.0000502.

[11] R.A. Stern, P. Koutrakis, M.A.G. Martins, B. Lemos, S.E. Dowd, E.M. Sunderland, E. Garshick, Characterization of hospital airborne SARS-CoV-2, Respir. Res. 22 (2021) 1–8, https://doi.org/10.1186/s12931-021-01637-8.

[12] G. Buonanno, L. Morawska, L. Stabile, Quantitative assessment of the risk of airborne transmission of SARS-CoV-2 infection : Prospective and retrospective applications, Environ. Int. 145 (2020), 106112, https://doi.org/10.1016/j.envint.2020.106112.

[13] C.K. Ho, Modeling airborne pathogen transport and transmission risks of SARS-CoV-2, Appl. Math. Model. 95 (2021) 297–319, https://doi.org/10.1016/j.apm.2021.02.018.

[14] R. Bhardwaj, A. Agrawal, How coronavirus survives for days on surfaces, Phys. Fluids 32 (11) (2020) 111706, https://doi.org/10.1063/5.0033306.

[15] R. Bhardwaj, A. Agrawal, Likelihood of survival of coronavirus in a respiratory droplet deposited on a solid surface, Phys. Fluids 32 (6) (2020) 061704, https://doi.org/10.1063/5.0012009.

[16] J.A. Otter, C. Donskey, S. Yezli, S. Douthwaite, S.D. Goldenberg, D.J. Weber, Transmission of SARS and MERS coronaviruses and influenza virus in healthcare settings: the possible role of dry surface contamination, J. Hosp. Infect. 92 (3) (2016) 235–250, https://doi.org/10.1016/j.jhin.2015.08.027.

[17] L. Xie, F. Liu, J. Liu, H. Zeng, A Nanomechanical Study on Deciphering the Stickiness of SARS- CoV - 2 on Inanimate Surfaces, ACS Appl. Mater. Interfaces 12 (52) (2020) 58360–58368, https://doi.org/10.1021/acsami.0c1680010.1021/acsami.0c16800.s001.

[18] R.A. Moreira, M. Chwastyk, J.L. Baker, H.V. Guzman, A.B. Poma, Quantitative determination of mechanical stability in the novel coronavirus spike protein, Nanoscale 12 (31) (2020) 16409–16413, https://doi.org/10.1039/D0NR03969A.

[19] X. Xue, J.K. Ball, C. Alexander, M.R. Alexander, All Surfaces Are Not Equal in Contact Transmission of SARS-CoV-2, Matter 3 (5) (2020) 1433–1441, https://doi.org/10.1016/j.matt.2020.10.006.

[20] J. Luque Di Salvo, G. De Luca, A. Cipollina, G. Micale, Effect of ion exchange capacity and water uptake on hydroxide transport in PSU-TMA membranes: A DFT and molecular dynamics study, J. Memb. Sci. 599 (2020) 117837, https://doi.org/10.1016/j.memsci.2020.117837.

[21] M.T. Degiacomi, V. Erastova, M.R. Wilson, Easy creation of polymeric systems for molecular dynamics with Assemble!, Comput. Phys. Commun. 202 (2016) 304–309, https://doi.org/10.1016/j.cpc.2015.12.026.

[22] M.J. Abraham, T. Murtola, R. Schulz, S. Páll, J.C. Smith, B. Hess, E. Lindahl, GROMACS: High performance molecular simulations through multi-level parallelism from laptops to supercomputers, SoftwareX 1-2 (2015) 19–25, https://doi.org/10.1016/j.softx.2015.06.001.

[23] W.L. Jorgensen, D.S. Maxwell, J. Tirado-Rives, Development and Testing of the OPLS All-Atom Force Field on Conformational Energetics and Properties of Organic Liquids, J. Am. Chem. Soc. 118 (45) (1996) 11225–11236, https://doi.org/10.1021/ja9621760.

[24] S. Farah, K.R. Kunduru, A. Basu, A.J. Domb, Molecular Weight Determination of Polyethylene Terephthalate, in: P.M. Visakh, M. Liang (Eds.), Poly(Ethylene Terephthalate) Based Blends, Compos. Nanocomposites, 2015, pp. 143–165, https://doi.org/10.1016/B978-0-323-31306-3.00008-7.

[25] M. Nofar, D. Sacligil, P.J. Carreau, M.R. Kamal, M. Heuzey, Poly (lactic acid) blends: Processing, properties and applications, Int. J. Biol. Macromol. 125 (2019) 307–360, https://doi.org/10.1016/j.ijbiomac.2018.12.002.

[26] A.C. Walls, Y. Park, M.A. Tortorici, A. Wall, A.T. Mcguire, D. Veesler, A.C. Walls, Y. Park, M.A. Tortorici, A. Wall, A.T. Mcguire, Structure, Function, and Antigenicity of the SARS-CoV-2 Spike Glycoprotein, Cell 180 (2020) 1–12, https://doi.org/10.1016/j.cell.2020.02.058.

[27] H. Woo, S.-J. Park, Y.K. Choi, T. Park, M. Tanveer, Y. Cao, N.R. Kern, J. Lee, M. S. Yeom, T.I. Croll, C. Seok, W. Im, Developing a Fully Glycosylated Full-Length SARS-CoV-2 Spike Protein Model in a Viral Membrane, J. Phys. Chem. B 124 (33) (2020) 7128–7137, https://doi.org/10.1021/acs.jpcb.0c0455310.1021/acs.jpcb.0c04553.s001.

[28] Y. Watanabe, J.D. Allen, D. Wrapp, J.S. McLellan, M. Crispin, Site-specific glycan analysis of the SARS-CoV-2 spike, Science 369 (6501) (2020) 330–333, https://doi.org/10.1126/science:abb9983.

[29] S. Grimme, J. Antony, S. Ehrlich, H. Krieg, A consistent and accurate ab initio parametrization of density functional dispersion correction (DFT-D) for the 94 elements H-Pu, J. Chem. Phys. 132 (2010) 154104–154119, https://doi.org/10.1063/1.3382344.

[30] M. Valiev, E.J. Bylaska, N. Govind, K. Kowalski, T.P. Straatsma, H.J.J. Van Dam, D. Wang, J. Nieplocha, E. Apra, T.L. Windus, W.A. de Jong, NWChem: A comprehensive and scalable open-source solution for large scale molecular simulations, Comput. Phys. Commun. 181 (9) (2010) 1477–1489, https://doi.org/10.1016/j.cpc.2010.04.018.

[31] M. Lund, B.o. Jönsson, A Mesoscopic Model for Protein-Protein Interactions in Solution, Biophys. J . 85 (5) (2003) 2940–2947, https://doi.org/10.1016/S0006-3495(03)74714-6.

[32] F. Petrosino, S. Curcio, S. Chakraborty, G. De Luca, Enzyme Immobilization on Polymer Membranes: A Quantum and Molecular Mechanics Study, Computation. 7 (2019) 1–9.

[33] S. Curcio, F. Petrosino, M. Morrone, G. De Luca, Interactions between Proteins and the Membrane Surface in Multiscale Modeling of Organic Fouling, J. Chem. Inf. Model. 58 (9) (2018) 1815–1827, https://doi.org/10.1021/acs.jcim.8b0029810.1021/acs.jcim.8b00298.s001.

[34] F. Petrosino, A multi-scale theoretical paradigm to model the complex interactions between macromolecules and polymeric membranes, PhD Thesis, Università della Calabria, Italy, 2020.
[35] W.D. Cornell, P. Cieplak, C.I. Bayly, I.R. Gould, K.M. Merz, D.M. Ferguson, D. C. Spellmeyer, T. Fox, J.W. Caldwell, P.A. Kollman, A Second Generation Force Field for the Simulation of Proteins, Nucleic Acids, and Organic Molecules, J. Am. Chem. Soc. 117 (19) (1995) 5179–5197, https://doi.org/10.1021/ja00124a002.
[36] K.N. Kirschner, A.B. Yongye, S.M. Tschampel, J. González-Outeiriño, C.R. Daniels, B.L. Foley, R.J. Woods, GLYCAM06: A Generalizable Biomolecular Force Field. Carbohydrates, J. Comput. Chem. 29 (2008) 622–655, https://doi.org/10.1002/jcc.20820.GLYCAM06.
[37] S. Senapati, A. Chandra, Dielectric Constant of Water Confined in a Nanocavity, J. Phys. Chem. B 105 (22) (2001) 5106–5109, https://doi.org/10.1021/jp011058i.
[38] H.V. Guzman, N. Tretyakov, H. Kobayashi, A.C. Fogarty, K. Kreis, J. Krajniak, C. Junghans, K. Kremer, T. Stuehn, ESPResSo++ 2.0: Advanced methods for multiscale molecular simulation, Comput. Phys. Commun. 238 (2019) 66–76, https://doi.org/10.1016/j.cpc.2018.12.017.
[39] L.-D. Chen, Effects of ambient temperature and humidity on droplet lifetime – A perspective of exhalation sneeze droplets with COVID-19 virus transmission, Int. J. Hyg. Environ. Health 229 (2020) 113568, https://doi.org/10.1016/j.ijheh.2020.113568.
[40] N.G. Di Novo, A.R. Carotenuto, G. Mensitieri, M. Fraldi, N.M. Pugno, Modeling of Virus Survival Time in Respiratory Droplets on Surfaces: A New Rational Approach for Antivirus Strategies, Front. Mater. 8 (2021) 1–13, https://doi.org/10.3389/fmats.2021.631723.
[41] B.W. Neuman, B.D. Adair, C. Yoshioka, J.D. Quispe, G. Orca, P. Kuhn, R. A. Milligan, M. Yeager, M.J. Buchmeier, Supramolecular Architecture of Severe Acute Respiratory Syndrome Coronavirus Revealed by Electron Cryomicroscopy, J. Virol. 80 (16) (2006) 7918–7928, https://doi.org/10.1128/JVI.00645-06.
[42] H. Yao, Y. Song, Y. Chen, N. Wu, J. Xu, C. Sun, J. Zhang, T. Weng, Z. Zhang, Z. Wu, L. Cheng, D. Shi, X. Lu, J. Lei, M. Crispin, Y. Shi, L. Li, S. Li, Molecular Architecture of the SARS-CoV-2 Virus, Cell 183 (3) (2020) 730–738.e13, https://doi.org/10.1016/j.cell.2020.09.018.
[43] Z. Ke, J. Oton, K. Qu, M. Cortese, V. Zila, L. McKeane, T. Nakane, J. Zivanov, C. J. Neufeldt, B. Cerikan, J.M. Lu, J. Peukes, X. Xiong, H.-G. Kräusslich, S.H. W. Scheres, R. Bartenschlager, J.A.G. Briggs, Structures and distributions of SARS-CoV-2 spike proteins on intact virions, Nature 588 (7838) (2020) 498–502, https://doi.org/10.1038/s41586-020-2665-2.